16th World Conference on Earthquake, 16WCEE 2017
Santiago Chile, January 9th to 13th 2017
Paper N° 636
Registration Code: S-F1462842672

S-WAVE IMPEDANCE MEASUREMENTS OF THE UPPERMOST MATERIAL IN SURFACE GROUND LAYERS

H. Goto(1), N. Tanaka(2), S. Sawada(3), and H. Inatani(4)

(1) *Associate Professor, Disaster Prevention Research Institute, Kyoto University, goto@catfish.dpri.kyoto-u.ac.jp*
(2) *Chemical Grouting, n-tanaka@chemicalgrout.co.jp*
(3) *Professor, Disaster Prevention Research Institute, Kyoto University, sawada@catfish.dpri.kyoto-u.ac.jp*
(4) *President, Katsujima Inc., inatani@katsujima.co.jp*

Abstract

S-wave impedance is one of the most effective parameters used to study the ground motion amplification of soil deposits. We propose a new approach to measure the S-wave impedance of the uppermost material in surface ground layers. First, a circular disk is set on the ground surface, and it is vertically loaded by sinusoidal wave excitation. When the time series of the loading velocity is synchronized with the reaction force, the ratio of the reaction force to the loading velocity is proportional to the S-wave impedance. We then estimate the proportionality coefficient from numerical experiments and check its accuracy. The measurement error is estimated to be within 1% for the homogeneous half-space case. We also discuss the applicability of this new approach and its limitations on the bases of numerical experiments for inhomogeneous media: a two-layered medium and a one-dimensional (1-D) random medium. The proposed approach is effective for both cases if we select the appropriate circular disk size.

Keywords: S-wave impedance; Site amplification; Geophysical exploration method

1. Introduction

Evaluating the risk of on earthquake disasters is one of the important issues in earthquake engineering. Quantification of ground motion amplification is an essential procedure in the risk analysis. In addition, the amplification due to the soil ground deposits directly caused severe damage to engineering structures during the past earthquakes. Several approaches have been proposed to quantify the amplification. Some of them have already been introduced into real-time systems that can estimate the impact of earthquake disasters [1]. These approaches are based on simple factors that classify the ground [2] via the averaged shear wave velocity, surface geology, geotechnical data, etc. Recently, Vs30, the averaged shear wave velocity to a 30m depth, has been widely adopted for site classifications [3]. Geomorphologic classifications [4] and topographic data [5,6,7] are used to evaluate Vs30 at sites where detailed velocity profiles are not available.

Some researchers, however, argue that Vs30 is not a significant parameter to model the site amplification [8,9]. However, the ratio of the S-wave impedance, that is, the product of S-wave velocity and density, was originally proposed to be the index to quantify the amplification. Joyner [10] pointed out that the amplification may be explained by the square root of the impedance ratio of rock to soil sites. Their idea has, unfortunately, not been readily accepted because they neglect the energy losses due to reflection at the material interface, which is essential to observe the resonance frequency of the surface ground. In recent research, the S-wave impedance was revived by Goto [11] in their analysis of the normalized energy density (NED). The NED is a single value model of the site amplification, but it integrates the frequency contents of the transfer function for the surface layer. The NED and average of the amplification are strongly correlated, which has been proven mathematically and numerically. In applications, the total damping in the surface ground can be directly estimated from the loss of the NED [12]. In order to evaluate the NED at a particular site, the S-wave impedance of the uppermost surface layer is an essential physical parameter to obtain, and it has to be measured by in situ field tests.

The S-wave impedance of the surface layer is also an important factor that is used to model soil-structure interactions. As reviewed by Kausel [13], a large amount of research has focused on these types of interactions, which have been reported since the end of the 19th century. Gazetas [14] summarized the approximate formulas of the dynamic stiffness and dashpot coefficient for various types of foundations. In his chart, the dashpot coefficient, which physically represents the radiation damping, is a function of the material impedance of the surface ground [15,16]. Because the impedance corresponds to the S-wave velocity or Lysmer's analog wave velocity, depending on the response directions, the S-wave impedance is a key parameter to model the dashpot coefficient of the foundations [17,18,19].

The S-wave impedance at the actual site has been estimated from the product of the measured S-wave velocity and density. The S-wave velocity profile is measured by various types of elastic wave explorations [21] such as PS logging, refraction surveys, reflection surveys [21,22], surface wave surveys [23], and microtremor array observations [24,25,26]. The density profile is measured from undisturbed soil samples or by density logging [27]. Although each technique has been well established, measurement errors and uncertainties still remain [28,29]. This may cause error propagation during estimation of the S-wave impedance. Thus, it is better to measure the S-wave impedance directly without the product.

Recently, direct estimation techniques of the material impedance for the subsurface structure have been developed in the field of exploration geophysics [30,31,32]. These techniques focus on the angle-dependent reflections from the material interface, and the dependence is estimated from the variation. These approaches are attractive, but they require several seismic records with a variety of angles. Because the body waves tend to travel vertically through the surface layers, a sufficient variation in the angles may not be available.

In this article, we briefly introduce our recent work, a new technique to measure the S-wave impedance on the uppermost surface layer [33]. We focus on the dynamic response of a rigid circular disk, which is placed on a target ground surface. The relations of the S-wave impedance and the ratio of the reaction force to the velocity at a synchronized frequency are described, and we then propose a procedure to estimate the S-wave impedance. Lastly, we present the results from two types of numerical experiments and verify the proposed technique.

2. Relation between disk velocity and reaction force on ground surface

Dynamic response of rigid circular disk placed on a surface of a half-space medium was analytically solved by Robertson [34]. He focused on the problem that the disk with a radius a was vertically excited by a sinusoidal oscillation (Fig.1). Reaction force acting to the disk $Pz(\omega)$ was provided, as follows:

$$\frac{Pz(\omega)}{\pi a^2} = \frac{4\mu u(\omega)}{\pi a(1-\upsilon)}[p_1(\omega) - ip_2(\omega)] \tag{1}$$

where μ and v are shear rigidity and Poisson ratio of the half-space medium, respectively. i is the imaginary unit. $p_1(\omega)$ and $p_2(\omega)$ are real functions. For the small angular frequency, p_1 and p_2 are approximated, as follows:

$$p_1(\omega) \sim 1 + \frac{1}{3\pi^2}(2\pi I_2 - 3I_1^2)\left(\frac{a\omega}{\beta}\right)^2 \tag{2}$$

$$p_2(\omega) \sim \frac{1}{\pi} I_1 \left(\frac{a\omega}{\beta}\right) \tag{3}$$

As increasing ω, $p_1(\omega)$ monotonically decreases, and $p_2(\omega)$ monotonically increases. Therefore, the root of $p_1(\omega) = 0$ exists. In substituting the root to Eq.(4), the reaction force is represented, as follows:

$$\frac{Pz(\omega)}{\pi a^2} = I_0 \rho\beta\dot{u}(\omega) \tag{4}$$

where ρ is a density. I_0 is a real coefficient depending on only v. Equation (3) suggests that the reaction force is proportional to the particle velocity when the reaction force is synchronized to the particle velocity. S-wave impedance $\rho\beta$ explicitly appears in the proportional coefficient.

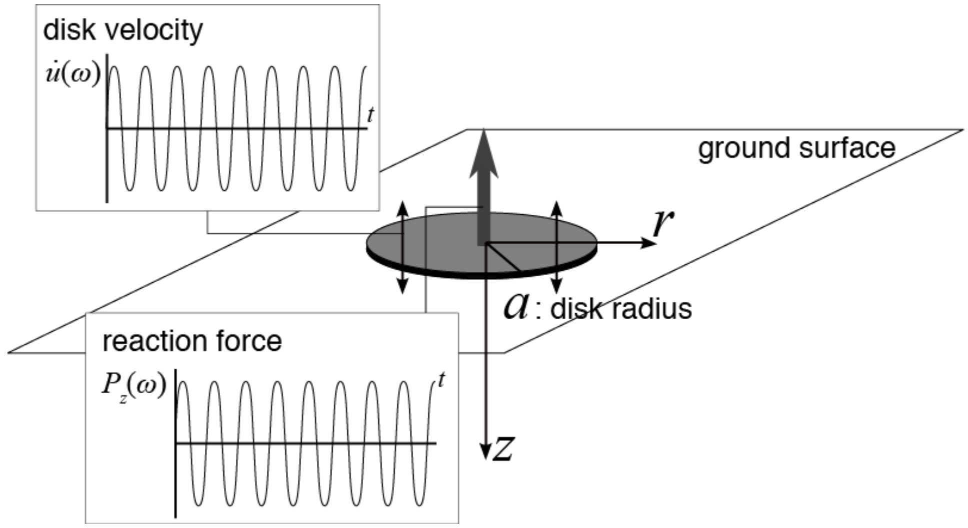

Fig. 1 – Schematic figure of vertical oscillation for rigid circular disk [33].

Robertson's solution is derived under the simple conditions; a homogeneous half-space medium, and stress free condition beneath the disk. In order to clarify the relation between the reaction force and the particle velocity, we numerically simulate the vertical oscillation of the rigid circular disk on the free surface.

Equation of motions for cylindrical coordinate with axial symmetry, and constitutive models for linear elasticity are applied. Finite element method is adopted to solve the boundary value problem. A finite domain is divided into 300×300 rectangular elements. 50 elements in horizontal direction are located beneath a half of the disk, $r \leq a$. 4-node isoparametric elements and explicit time integration are used. The time steps are 0.01 times the maximum P-wave velocity in the domain. To model the excitation by the rigid disk, the forced displacement ($u(\omega)$, 0) is explicitly applied on the nodes located in $r \leq a$. on the top edge. 1-D non-reflecting boundary conditions are allocated on the artificial boundaries, side and bottom edges of the domain.

The coefficient I_0 is numerically evaluated from Eq.(3). Figure 2 shows the coefficient for all the simulated cases. For the reference, the value of I_0 for $\nu = 0.50$ by Robertson is also plotted. The results indicate that the coefficient is not well correlated to S-wave velocity, Poisson ratio, and density, excepting the case $\nu = 0.40$, although the original I_0 depends on the Poisson ratio. The main reason is the constraint beneath the disk because the Poisson effect is restricted. The results in Fig.2 also indicate the ratio of the average reaction force to the particle velocity is proportional to the S-wave impedance with the unique proportional coefficient I_0. The average of the coefficients among the results in cases $\nu = 0.45, 0.48, 0.49$ is 2.2788, which may be applicable to all the cases. Then, we propose to commonly use $I_0 = 2.2788$. Figure 3 shows the comparison of the estimated S-wave impedance by using $I_0 = 2.2788$ to the material (true) one in all the cases. The estimated S-wave impedances are almost equal to the true ones, excepting $\nu = 0.40$ case. A standard deviation of the estimation error for $\nu \geq 0.41$ cases is 0.99%, which is quite accurate to measure the S-wave impedance. The original coefficient by Robertson requires the Poisson ratio, which is unknown variable, whereas we can apply $I_0 = 2.2788$ universally independent of the Poisson ratio. It is an efficient property in the measurement.

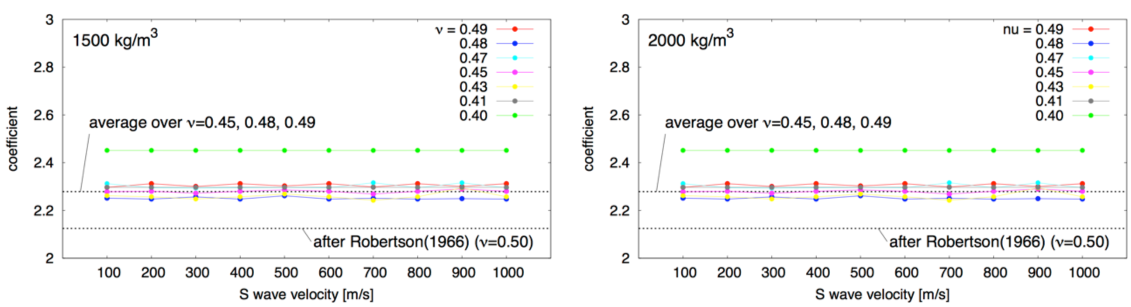

Fig. 2 – Coefficient I_0 evaluated from variable types of numerical experiments [33].

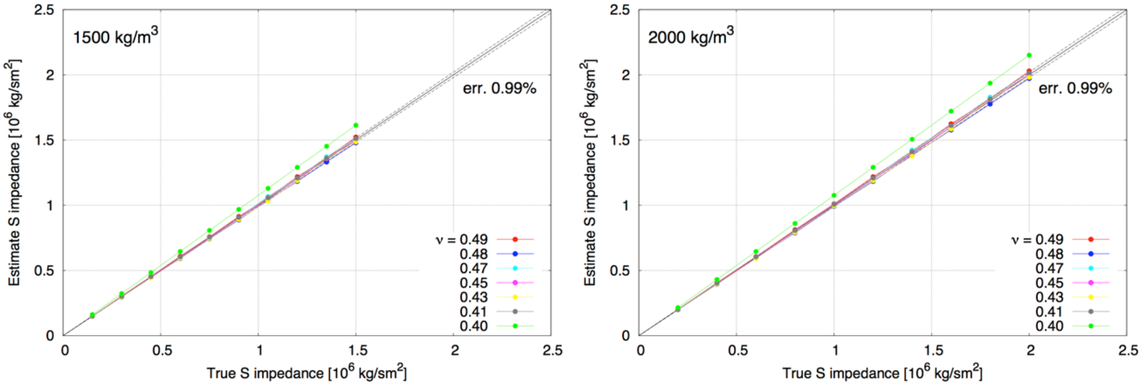

Fig. 3 – Comparison of estimated S-wave impedance to the true one by using coefficient I_0 = 2.2788 [33].

3. Measurement procedure for the S-wave impedance

On the basis of the properties of the relation between the disk velocity and the reaction force acting on the rigid circular disk, we propose a simple procedure to measure the S-wave impedance of the uppermost layer of the surface ground [33].

Step 1. A rigid circular disk is vertically loaded at variable frequencies, and the reaction force and disk velocity are measured. We set a rigid circular disk on the ground surface and vertically load it by sinusoidal wave excitation with a variety of frequencies (see Fig. 1). The reaction force acting on the disk and the disk velocity are measured for each frequency.

Step 2. The synchronized frequency between the reaction force and the disk velocity is determined. The time series of the measured reaction force is compared to the one for the disk velocity, and their phase difference is calculated. The excitation frequency with zero phase difference is then determined and set to the synchronized frequency.

Step 3. The ratio of the averaged reaction pressure to the disk velocity at the synchronized frequency is calculated. The amplitude of the averaged reaction pressure, which is defined by $Pz/\pi a^2$ is divided by the amplitude of the disk velocity at the synchronized frequency. The value is set to the measured ratio.

Step 4. The ratio is divided by I_0=2.2788, and then, the S-wave impedance is obtained. As shown in Fig. 2, the measured ratio divided by the material S-wave impedance is constant independent of the material properties, and it is modeled with the value of I_0=2.2788. Therefore, the measured ratio is divided by 2.2788, and we can then obtain the S-wave impedance of the uppermost surface layer at the target site.

If horizontal loadings to the circular disk are required in the procedure, we must ensure strong coupling to the contact surface to prevent slippage between the disk and the ground surface. The procedure used here, fortunately, requires only vertical loadings to estimate the S-wave impedance. This allowed us to realize the loading system without having to implement special treatments to the contact surface.

The proposed procedure was verified in a homogeneous half-space medium, even though the natural ground surface cannot be assumed to be a homogeneous half-space. Therefore, in order to clarify the effects of the material interfaces and inhomogeneity, we demonstrate the measured procedure for more general media through two numerical experiments.

4. Numerical experiment

4.1 Two-layered medium

We first clarify the effect of the material interfaces by performing numerical experiments on a two-layered medium, which consists of a single surface layer overlying a homogeneous half-space basement. The physical parameters of both the surface layer and basement are presented in Table 1. We evaluated three cases with variable surface layer thicknesses of 0.5m, 1.0m, and 2.0m and the half-space case as a reference. The Poisson ratios of the surface layer and basement were 0.493 and 0.43, respectively, which are in the applicable range of I_0=2.2788.

Table 1 – Physical parameters for the two-layered medium.

	Surface layer	Basement
S-wave velocity [m/s]	180	700
P-wave velocity [m/s]	1500	2000
Density [kg/m^3]	1400	1600
Thickness [m]	0.5, 1.0, 2.0, ∞	–

For the half-space medium, the results were independent of the disk radius. However, for the two-layered medium, a relation between the disk radius and the surface layer thickness was apparent. We performed numerical experiments by applying seven disk radii for each case: 0.1m, 0.2m, 0.5m, 1.0m, 2.0m, 5.0m, and 10.0m. In order to ensure 50 elements beneath each disk size, the size of the elements was modified in each simulation of the disk radius. We then applied the proposed procedure described in the previous section to estimate the S-wave impedance. We omit the case for a disk radius of 0.1m and a thickness of 2.0m because the thickness exceeds the vertical dimension of the entire domain. For the other cases, the relative element sizes to the wavelength is ensured to be sufficiently small, e.g., 25 elements represent the wavelength at the synchronized frequency for a disk radius of 10m and a thickness of 0.5m.

Figure 4 shows the S-wave impedances estimated from the various disk radii. The black solid lines indicate the true S-wave impedances in the surface layer and basement. For small disk radii, namely, 0.1-0.2m, the estimated S-wave impedances agreed well with the S-wave impedances of the surface layer. However, the values were underestimated at a radius of approximately 1m, and they increased to the S-wave impedance of the basement as the radius increased. The small disk size generates a wave field that mainly consists of shorter wavelengths at the synchronized frequency. In one example, the wavelength for a disk radius of 0.2m and a thickness of 1.0m is 0.57m, which is half of the surface layer thickness. The table also implies that a wavelength shorter than the layer thickness gives almost the same synchronized frequencies as the half-space case. Therefore, the effect from the layer boundary depends on the relative size of the disk to the layer thickness.

To enhance the relative thickness to the disk radius, we plotted the estimated values associated with a normalized disk radius, which was defined by the disk radius divided by the surface layer thickness, in Fig. 4. This clearly shows that all cases are on a common curve, and the minimum value appears when the disk radius is equal to the surface layer thickness. This implies that the S-wave impedances estimated from approximately 20% size of the disk radius relative to the surface layer thickness must be correct. In general, we did not have much information about the layer thickness at the target site, but several experiments with a variety of disk radii will give a curve similar to that shown in Fig. 4, and this will give an appropriate value of the S-wave impedance as a limiting value for shorter disk sizes.

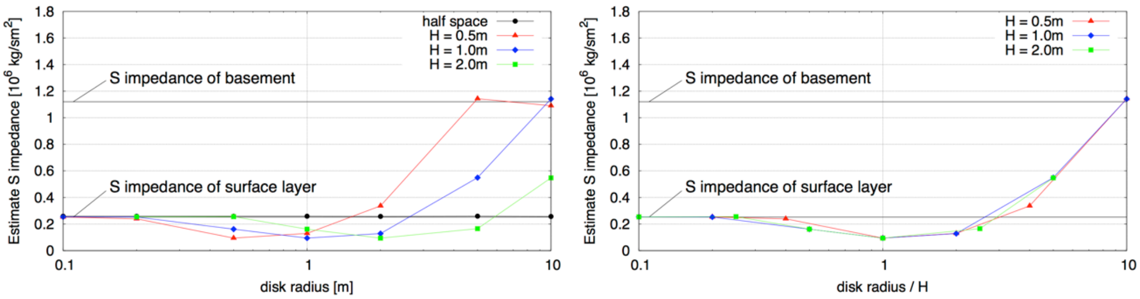

Fig.4 – Estimated S-wave impedance for two-layered media plotted with a disk radius and a normalized disk radius [33].

4.2 1-D random medium

Natural materials that compose the ground surface usually have variable material properties. We performed another numerical experiment for more complex layered structures in order to check the robustness of the proposed method.

The variations in velocities and densities were applied only to the depth direction, and they were modeled by adding fluctuations to the average model. Table 2 summarizes the parameters for the average model, which is based on 1-D profiles at the K-NET MYG006 seismic station maintained by the National Research Institute for Earth Science and Disaster Prevention (NIED). Severe residential damage around the K-NET MYG006 site was concentrated during the 2011 off the Pacific coast of Tohoku earthquake [35]. The detailed soil profiles have been investigated from the very dense observations of strong ground motions [36], and the soft soil deposit is estimated to a depth of approximately 15-30m. Although there are no significant reasons to adopt the profile at the K-NET MYG006 site in this study, we choose a target site covered with the soft soil deposit because large site amplification is expected.

Table 2 – Average model for the one-dimensional (1-D) random medium.

	Surface layer #1	Surface layer #2	Basement
S-wave velocity [m/s]	70	130	400
P-wave velocity [m/s]	350	1420	1880
Density [kg/m^3]	1425	1750	2110
Thickness [m]	2.0	15.0	–

We adopted the von Kármán autocorrelation function and applied it to the fluctuations [37]. In the experiments, correlation distance a and order of modified Bessel function κ were set to 10m and 0.5, respectively. Two cases of mean square fractional fluctuation ε^2, 0.02 and 0.1, were examined. We generated 10 samples and performed numerical experiments for each case.

A 0.2m disk radius was applied, and we then obtained simulation results using the measurement procedure for the S-wave impedance. Figure 5 shows the estimated S-wave impedance from the 1-D random medium. The horizontal axis corresponds to the sample number of the random model. Because the S-wave impedance of surface layer #1 contains fluctuations, the ranges of the standard deviation and minimum-maximum values are also plotted in Fig. 5. All estimated values were in the range of the minimum-maximum values of the model for ε^2=0.02, and almost all of the cases were in the range of the standard deviation. For the strong fluctuation case (ε^2=0.1), the estimated value for one of the samples (sample 4) was outside the range of the minimum--maximum values. However, the estimates for over half of the cases were in the range of the standard deviation.

This implies that the proposed method gives accurate estimates of the S-wave impedance of the uppermost surface layer, even when the material includes some fluctuations.

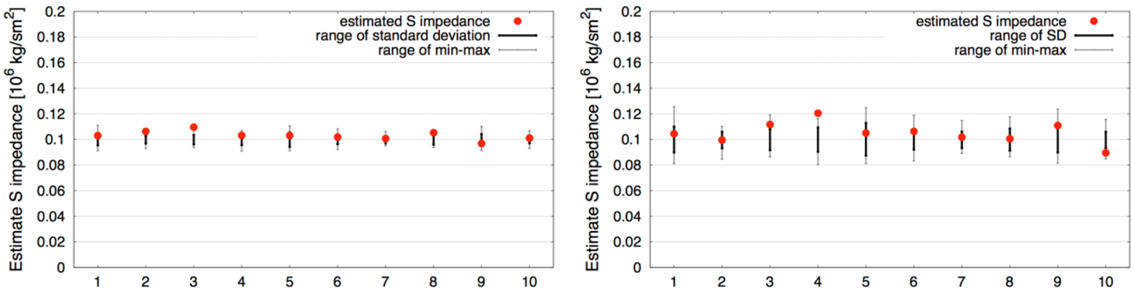

Fig.5 – Estimated S-wave impedance for each 10 sample model (left: $\varepsilon^2 = 0.02$, right: $\varepsilon^2 = 0.1$) [33].

5. Conclusion

In this study, we proposed a new approach to measure the S-wave impedance in the uppermost surface layer. A rigid circular disk is set on a free surface, and it vertically oscillates as it synchronizes with the reaction force and disk velocity. The ratio of the averaged reaction pressure to the velocity is a product of the S-wave impedance and a coefficient estimated as I_0=2.2788. The S-wave impedance estimated from the procedure is quite accurate in numerical experiments for a homogeneous half-space medium. For the two-layered medium, the estimated value is appropriate when a small disk radius is selected. For the 1-D random medium, the proposed approach gives accurate estimates compared to the variation itself.

Important issues of the future research are the effective depth of the estimated S-wave impedance at the actual soil ground. We are going on the laboratory tests and field tests as the implementation of this theory. In addition, we now study the effective factors to site amplification will be discussed based on the observed records, especially compared in comparison to Vs_{30}.

6. Acknowledgements

The research was supported by a Grant-in-Aid for Young Scientists from the Japan Society for the Promotion of Science (JSPS) (No. 25709039).

7. References

[1] Wald DJ, Jaiswal KS, Marano KD, Bausch DB, Hearn MG (2010): PAGER – Rapid assessment of an earthquake's impact. *U.S. Geological Survey Fact Sheet 2010-3036*.

[2] Bouzorgnia Y, Bertero VV (2004): *Earthquake Engineering from Engineering Seismology to Performance-Based Engineering*. CRC Press.

[3] Borcherdt RD (1994): Estimates of site–dependent response spectra for design (methodology and justification). *Earthquake Spectra*, **10** (4), 617-653.

[4] Wakamatsu K, Matsuoka M (2006): Development of the 7.5-arc-second engineering geomorphologic classification database and its application to seismic microzoning. *Bull. Earthquake Res. Inst., University of Tokyo*, **81**, 317-324.

[5] Wald DJ, Allen TI (2007): Topographic slope as a proxy for seismic site conditions and amplification. *Bull. Seism. Soc. Am.*, **97** (5), 1379-1395.

[6] Allen TI, Wald DJ (2009): On the use of high-resolution topographic data as a proxy for seismic site conditions (VS30). *Bull. Seism. Soc. Am.*, **99** (2A), 935-943.

[7] Thompson EM, Wald DJ, Worden CB (2014): A VS30 map for California with geologic and topographic constraints. *Bull. Seism. Soc. Am.*, **104** (5), 2313-2321.

[8] Castellaro S, Mulargia, F, Rossi PL (2008): Vs30: Proxy for seismic amplification? *Seism. Res. Lett.*, **79** (4), 540-543.

[9] Lee VW, Trifunac MD (2010): Should average shear-wave velocity in the top 30\,m of soil be used to describe seismic amplification? *Soil Dyn. Earthquake Eng.*, **30** (11), 1250-1258.

[10] Joyner WB, Warrick RE, Fumal TE (1981): The effect of quanternary alluvium on strong ground motion in the Coyote lake, California, earthquake of 1979. *Bull. Seism. Soc. Am.*, **71** (4), 1333-1349.

[11] Goto H, Sawada S, Hirai T (2011): Conserved quantity of elastic waves in multi-layered media: 2D SH case – Normalized Energy Density–. *Wave Motion*, **48** (7), 603-613.

[12] Goto H, Kawamura Y, Sawada S, Akazawa T (2013): Direct estimation of near-surface damping based on normalized energy density. *Geophys. J. Int*., **194** (1), 488-498.

[13] Kausel E (2010): Early history of soil-structure interaction. *Soil Dyn. Earthquake Eng.*, **30** (9), 822-832.

[14] Gazetas G (1991): Formulas and charts for impedances of surface and embedded foundations. *J. Geotech. Engrg.*, **117** (9), 1363-1381.

[15] Gazetas G, Dobry R (1984): Simple radiation damping model for piles and footings. *J. Eng. Mech.*, **110** (6), 937-956.

[16] Gazetas G, Tassoulas JL (1987): Horizontal damping of arbitrarily shaped embedded foundations. *J. Geotech. Engrg.*, **113** (5), 458-475.

[17] Wolf JP, Somaini DR (1986): Approximate dynamic model of embedded foundation in time domain. *Earth. Eng. Struct. Dyn.*, **14** (5), 683-703.

[18] Wolf JP (1997): Spring-dashpot-mass models for foundation vibrations. *Earth. Eng. Struct. Dyn.*, **26** (9), 931-949.

[19] Gerolymos N, Gazetas G (2006): Winkler model for lateral response of rigid caisson foundations in linear soil. *Soil Dyn. Earthquake Eng.*, **26** (5), 347-361.

[20] Boore DM (2006): Determining subsurface shear-wave velocities: a review. *Proc. of 3rd International Symposium on the Effects of Surface Geology on Seismic Motion*, 103.

[21] Allen SJ (1980): Seismic method. *Geophysics*, **45** (11), 1619-1633.

[22] Yokokura T (1995): Research and development on the multi-channel seismic reflection method and its applications to various geological situations in Japan. *J. Phys. Earth*, **43** (3), 321-349.

[23] Park CB, Miller RD, Xia J (1999): Multichannel analysis of surface waves. *Geophysics*, **64** (3), 800-808.

[24] Aki K (1957): Space and time spectra of stationary stochastic waves, with special reference to microtremors. *Bull. Earthquake Res. Inst., University of Tokyo*, **35** (3), 2313-2321.

[25] Aki K (1965): A note on the use of microseisms in determining the shallow structure of the Earth's crust. *Geophysics*, **30** (4), 665-666.

[26] Okada H (2003): *The Microtremor Survey Method*. Society of Exploration Geophysicists.

[27] Jia R, Hino T, Chai J, Hamada T, Yoshimura M (2013): Interpretation of density profile of seabed sediment from nuclear density cone penetration test results. *Soils and Foundations*, **53** (5), 671-679.

[28] Liu HP, Boore DM, Joyner WB, Oppenheimer DH, Warrick RE, Zhang W, Hamilton JC, Brown LT (2000): Comparison of phase velocities from array measurements of Rayleigh waves associated with microtremor and results calculated from borehole shear-wave velocity profiles. *Bull. Seism. Soc. Am*., **90** (3), 666-678.

[29] Boore DM, Thompson EM (2007): On using surface-source downhole-receiver logging to determine seismic slownesses. *Soil Dyn. Earthquake Eng.*, **27** (11), 971-985.

[30] Connolly P (1999): Elastic impedance. *The Leading Edge*, **18** (4), 438-452.

[31] Whitcombe DN (2002): Elastic impedance normalization. *Geophysics*, **67** (1), 60-62.

[32] Lu S, McMechan GA (2004): Elastic impedance inversion of multichannel seismic data from unconsolidated sediments containing gas hydrate and free gas. *Geophysics*, **69** (1), 164-179.

[33] Goto H, Tanaka N, Sawada S, Inatani H (2015): S-wave impedance measurements of the uppermost material in surface ground layers: vertical load excitation on a circular disk. *Soils and Foundations*, **55** (5), 1282-1292.

[34] Robertson IA (1966): Forced vertical vibration of a rigid circular disc on a semi-infinite elastic solid. *Math. Proc. Camb. Phil. Soc.*, **62** (3), 547–553.

[35] Goto H, Morikawa H (2012): Ground motion characteristics during the 2011 off the Pacific coast of Tohoku earthquake. *Soils and Foundations*, **52** (5), 769-779.

[36] Goto H, Morikawa H, Inatani M, Ogura Y, Tokue S, Zhang XR, Iwasaki M, Araki M, Sawada S, Zerva A (2012): Very dense seismic array observations in Furukawa district, Japan. *Seismological Research Letters*, **83** (5), pp.765-774.

[37] Sato H, Fehler MC, Maeda T (2012): *Seismic Wave Propagation and Scattering in the Heterogeneous Earth: Second Edition*, Springer.